Biointerface Research in Applied Chemistry
Open-Access Journal (ISSN: 2069-5837)

Article
Volume 13, Issue 5, 2023, 478
https://doi.org/10.33263/BRIAC135.478

An Eco-Friendly Water Treatment Biofilm Based on Chitosan-Starch Blend with Natural Extracts: Red Radish and Pomegranate

Mildred M. Navarro-Reyes [1], Nancy P. Diaz-Zavala [1,*], Josue F. Perez-Sanchez [2,*], Beatriz I. Tijerina-Ramos [1], Jaime E. Sosa-Sevilla [1]

[1] Instituto Tecnológico de Ciudad Madero, Tecnológico Nacional de México, Ciudad Madero, Tamaulipas, Mexico; G15071550@cdmadero.tecnm.mx (M.M.N.-R.); nancy.dz@cdmadero.tecnm.mx (N.P.D.-Z.); beatriz.tr@cdmadero.tecnm.mx (B.I.T.-R.); jaime.ss@cdmadero.tecnm.mx (J.E.S.-S.);
[2] Facultad de Arquitectura, Diseño y Urbanismo, Universidad Autónoma de Tamaulipas, Tampico, Tamaulipas, Mexico; josue.perez@uat.edu.mx (J.F.P.-S.);
* Correspondence: nancy.dz@cdmadero.tecnm.mx (N.P.D.Z.); josue.perez@uat.edu.mx (J.F.P.S.);
Scopus Author ID 56006641400 (N.P.D.Z.)
57200005825 (J.F.P.S.)

Received: 26.09.2022; Accepted: 30.10.2022; Published: 3.01.2023

Abstract: Global water crisis is a topic that requires the development of methods that ensure water cleaning without residue generation. Chitosan-starch blend dopped with different natural extracts or inorganic compounds is broadly applied for water remediation. In this work, a series of chitosan-starch biofilms were produced with the addition of red radish and pomegranate extracts. The study was conducted using formic and acetic acid to determine the effect of the acid on materials integration and biofilm properties. It was found that acetic acid produces films with higher tensile strength and weathering resistance. However, formic acid performs a better antimicrobial activity and BOD and COD control when mixed with red radish anthocyanins. The chloride ion interaction had better results for those films produced with formic acid. Future work will pursue formulations combining the four elements: formic acid, acetic acid, red radish extract, and pomegranate extract, to improve the resistance of the biofilms, maintain the antimicrobial activity, the retention of organic material, and interact with salts ions for achieving water treatment at significant scale.

Keywords: chitosan-starch composite; red radish and pomegranate anthocyanins; antimicrobial films; chloride ion capture; water remediation

1. Introduction

The global water crisis has overcome us. Nowadays, many cities on all continents have a challenging issue with water supply [1-3], without mentioning the constant water crisis in the Middle East [4,5]. Mexico is not the exception, and the water crisis has exponentially arisen because of the rupture of marsh borders, resulting in the mixing of fresh and saltwater [6,7]. Among the several water treatment methods, some focus on sustainable materials or processes that look to accomplish water purification and avoid residual production [8-10].

The use of films and biofilms is one of the most studied methods. Chitosan-starch blend dopped with different natural extracts or inorganic compounds is broadly applied for water remediation and other medical and food applications [11-14]. In this work, red radish (*Raphanus sativus*) and pomegranate (*Punica granatum*) extracts were used to enhance the

microbiological properties of chitosan-starch films. Anthocyanins from red radish and pomegranate have been mainly applied as antioxidants to prevent food decomposition, as colorants, or as sensors for different applications [15-22]. This research was conducted to study the effect of the extracts on the antimicrobial capacity, biochemical oxygen demand (BOD) and chemical oxygen demand (COD) reduction, and chloride ion (Cl^-) capture in aqueous media, having as substrate chitosan-starch films.

2. Materials and Methods

The methodology was subdivided into three stages: obtention of natural extracts, biofilms production, and application tests. Two different acids were used to qualify the integration of the chitosan-starch blend.

2.1. Materials.

From Sigma-Aldrich: Chitosan (85%) deacetylated medium molecular weight, starch from rice, hydrochloric acid fuming (37%), ethanol HPLC, tartaric acid (99%), deuterated water, and tetramethylsilane. From Fermont: Glacial acetic acid (99.9%), formic acid (95%), glycerol (99.7%), and sulphuric acid (98%). From BD Bioxon: Potato dextrose agar, violet red bile agar, and agar-agar. From JT Baker: sodium chloride, silver nitrate, and potassium chromate. Sodium hydroxide was purchased from Merck and deionized; distilled water was purchased from Hycel.

2.2. Obtention and characterization of natural extracts.

Pomegranate extract was obtained with a food processor from the entire fruit. The blend was filtered to remove fiber residuals and centrifugated at 6000 rpm for 20 min. The supernatant was stored at 5°C. For radish extract, 100 g of red radish peel was mixed with 200 mL of an acidic aqueous solution (HCl 1%) with ethanol (50:50). The mixture was blended and filtered to eliminate coarse particles. The liquid phase was centrifugated at 6000 rpm (20 min), and the supernatant was aged for 24 h at 5 °C. After aging, some sedimentable particles were observed, and the centrifugation process was repeated until there were no fine particles.

After obtention, the natural extracts were analyzed to determine the total anthocyanin content with a UV-Vis spectrophotometer (Agilent Cary 60). The extracts were adjusted to pH=1 with HCl 4 N. 250 µL of each one was diluted in 12 mL of acidic ethanol (ethanol/HCl 1N 85:15) and centrifugated at 6000 rpm (40 min). The mixtures were gauged to 25 mL with acidic ethanol and manually mixed before analysis. The total anthocyanin content of each source was calculated with Equations 1 and 2, respectively [23,24]. For pomegranate, the total anthocyanin was determined as cyanidin 3-glucoside:

$$C_1 = MW \times 10^6 \left(\frac{A_1}{\varepsilon_1}\right)\left(\frac{V}{1000}\right)\left(\frac{1}{m}\right) \quad (1)$$

where C_1 is the concentration of total anthocyanin (mg/kg), MW is the molecular weight of cyanidin 3-glucoside (449 g/mol), A_1 is absorbance (at 535 nm), ε_1 is molar absorptivity of cyanidin 3-glucoside (25.965 $cm^{-1}M^{-1}$), V is the total volume of anthocyanin extract, and m is sample weight (g). The anthocyanin content in the red radish extract was calculated using the following equation, adjusting pH to 1 and 4,5:

$$C_2 = (A_2 \times MW \times 10^3)\left(\frac{1}{\varepsilon_2 \times L}\right) \quad (2)$$

where C_2 is the concentration of total anthocyanin (mg/L), A_2 is the absorbance at 510 nm for pH 1,0 minus the absorbance at 510 nm for pH 4,5, MW is the anthocyanin molecular weight (433,2 g/mol), ε_2 is the extinction coefficient (31.600 $Lcm^{-1}mol^{-1}$), and L is the path length (1 cm).

Extracts were also analyzed through NMR in a Bruker Ascend 400 system @400 MHz with 30° pulses (16 scans/s at 25 °C). H^1 and C^{13} were obtained from 30 mg/0,55 mL D_2O solution.

2.3. Biofilm production.

The chitosan-starch blend was produced from the precursor solutions of the materials. Chitosan precursor started with 1 L of an aqueous solution with acetic or formic acid (1% v/v). 20 g of chitosan was added to each solution and mixed under mechanical stirring for 24 h. The starch precursor started with 1 L of water heated at 90 °C, in which 20 g of rice starch was added under constant stirring for 20 min or until no grume observation and then cooled to ambient temperature. The rheological behavior of biopolymer solutions was studied in a rotational rheometer with temperature control (Anton Paar Rheolab QC) at a shear rate of 50 1/s for temperatures 20, 25, 30, 35, 40, and 45 °C. Then, the films were produced from an 80 mL mixture according to the quantities shown in Table 1. Natural extracts were added in 0,4 mL, 1,6 mL, and 4 mL. In all cases, 0,25 mL of glycerol was added to the mixture [11,25-27].

Table 1. Experimental design for the biofilm blends where A=acetic acid, F=formic acid, P=pomegranate extract, and R=red radish extract, in %v/v.

ID	Chitosan (C)	Starch (S)	Glycerol	Extract
CSA	49,9	49,9	0,25	0
CSAP0,5	49,65	49,65	0,25	0,5
CSAP2	48,9	48,9	0,25	2
CSAP5	47,4	47,4	0,25	5
CSAR0,5	49,65	49,65	0,25	0,5
CSAR2	48,9	48,9	0,25	2
CSAR5	47,4	47,4	0,25	5
CSF	49,9	49,9	0,25	0
CSFP0,5	49,65	49,65	0,25	0,5
CSFP2	48,9	48,9	0,25	2
CSFP5	47,4	47,4	0,25	5
CSFR0,5	49,65	49,65	0,25	0,5
CSFR2	48,9	48,9	0,25	2
CSFR5	47,4	47,4	0,25	5

The mixtures were poured on XPS plates (220 x 97 mm) and aged in darkness for three weeks under temperature and humidity-controlled conditions (23 °C, 30-50% RH) to form the films in triplicate. Once created, the mechanical, optical, and durability properties of biofilms were determined.

The thickness was measured for each film in five points, as shown in Figure 1a. The thickness was reported as the average (mm), and tests were performed with an OBI brand handheld micrometer model 264105 with a measuring range of 0 to 25 mm. First, tensile strength was determined with a Universal Machine (Controls). Then, the films were fitted to 60 x 30 mm probes and glued with epoxy resin on the edges (Figure 1b). According to the thickness measured, tensile strength was calculated with Equation 3, where σ is the tensile strength in N/m^2, P is the applied load in N, and A is the transversal cross-section in m^2.

$$\sigma = \frac{P}{A} \quad (3)$$

(**a**) (**b**)

Figure 1. (**a**) Thickness measuring points; (**b**) tensile strength test.

The accelerated weathering test was performed to determine the capacity of the biofilms to resist ambient exposure conditions in terms of solar light (UV radiation and temperature) and humidity (rain and dew). A QUV Spray Tester (QLab) was used with UVA-340 fluorescent lamps (340 nm @ 0,77 W/m^2/nm) to reproduce solar light at 60 °C and 100% relative humid at 50 °C, following the ASTM-G154 time parameters: 8 h UV (60 ± 3 °C) plus 4 h condensation (50 ± 3 °C). The weathering test was complemented with polarizable light microscopy (Motic BA210 4-10x) to observe the surface changes before and after the degradation assay. Also, mass films were recorded before and after the accelerated weathering test.

2.3. Application tests.

Once characterized, the biofilms were tested against aerobic mesophilic (AM), total coliforms (TC), fungi (Fg), reduction of BOD and COD, and the retention of Cl^- in aqueous media. The microbiological tests were based on the discs method from Bauer and Kirby [28-30]. Three probes of 6 mm diameter were obtained from each film and then pasteurized at 70 °C for 30 min. The probes were cultivated through the antibiogram method with a loop employing the following cultivation media: standard agar for AM, violet red bile agar for TC, and potato dextrose agar for Fg. All materials were sterilized (dry ambient) at 150 °C for 2 h. Table 2 shows the composition of the cultivation media.

Table 2. Cultivation media preparation.

Media	Aqueous solution	Heating dilution	Sterilization
Standard agar (SA)	2,35 g / 100 mL	100 °C / 1 min	15 psi / 15 min
Violet red bile agar (VRA)	41,50 g / 1000 mL	100 °C / 1 min	15 psi / 15 min
Potato dextrose agar (PDA)	39,00 g / 1000 mL	100 °C / 1 min	15 psi / 15 min

For AM and TC, a cheese sample was used as a bacteria source with 1 g of biomass solution in 10 mL of water, taking 1 mL (AM) and 0,1 mL (TC) aliquots for inoculation. The media was spread by moving seven times up, down, left, and right directions; then incubated at 37 °C for 24 h [31,32]. For the Fg test, 1,4 mL of an aqueous solution of tartaric acid (10%) was added for every 100 mL of PDA solution to reach a pH value of 3,5. *Aspergillus niger* was the fungus selected for the test, and a sample was suspended in 10 mL of water, from which 0,1 mL was placed on the plates. The media was also spread by moving seven times up, down, left, and right directions; then incubated at 25 °C for 120 h [33]. After incubation, samples were analyzed by visual inspection (Figure 2).

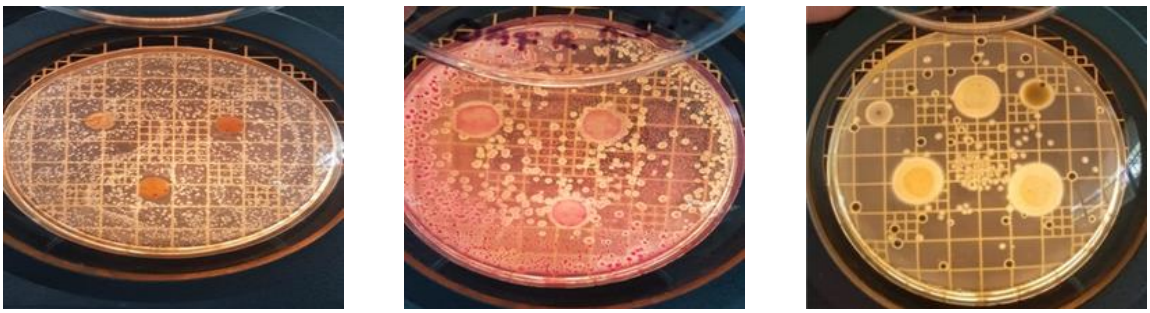

(**a**) (**b**) (**c**)

Figure 2. Examples of the microbiologic tests for (**a**) aerobic mesophilic, (**b**) total coliforms, and (**c**) fungi.

BOD and COD were performed with a sample of water extracted from lagoon "El Conejo" in Altamira, Tamaulipas, Mexico, a water body in the middle of an industrial zone (22°25'41,4 "N, 97°53'00,2 "W). The pH of 4 L of water was neutralized (6 to 8) with sulfuric acid 0.1 N for BOD, and 4 L was acidified (pH=2) for the COD test. After sampling, the water was maintained at 4 °C until experimentation [34,35]. The biofilms were cut into 50 x 35 mm probes for this test and placed into 100 mL of lagoon water for BOD or COD, respectively, at 20 °C. Every 20 min, under constant stirring, a 10 mL aliquot was taken and diluted to 100 mL with distilled water.

For BOD [36], after the interaction with the films, water samples were kept at 20 °C and pH adjusted (6,5 to 7,5) with H_2SO_4 or NaOH 0,1 N, respectively, and diluted in inoculated water (300 mL) at 1, 5, and 20% v/v in Winkler bottles. Dissolved oxygen was determined with a Corning potentiometer Pinnacle 555 and an oxygen electrode Orion 97-08-99 before and after five incubation days at 20 °C. BOD was calculated as shown in Equation 4, where R_1 and R_2 are the initial and final oxygen readings, and %D is the dilution percentage. DF is the dilution factor that corresponds to 10.

$$BOD_5\left(\frac{mg}{L}\right) = \frac{R_1 - R_2}{\%D} \times 100 \times DF \quad (4)$$

COD was determined as described in [37] by applying the spectrophotometric method. To this end, a five-point calibration curve was obtained from 20 to 220 mg/mL of O_2 equivalent to potassium biphthalate. First, 2,5 mL of lagoon water treated with biofilms was mixed with 1,5 mL digestion solution (Table 3) in reaction tubes. After cooling the reaction, 3,5 mL of digestion solution was added to the pipes, and the last ones were placed in a digestor system at 150 °C (2 h). After digestion, samples and calibration curve points were cooled to 25 °C and recorded by UV-Vis @ 600 nm.

Table 3. Specifications of digestion solutions for COD analysis.

Expected COD	Solution	$K_2Cr_2O_7$	H_2SO_4	$HgSO_4$	Dilution in water
> 75 mg/L	A	10,216 g	167 mL	33,3 g	1000 mL
5 to 75 mg/L	B	1,0216 g	167 mL	33,3 g	1000 mL

The water-film interaction method was also applied to determine the Cl^- retention. In this case, the Mohr methodology [38] was used for two chloride ion sources: NaCl aqueous solution 0.0014 N and seawater sampled from the litoral of the Gulf of Mexico, 30 m out to sea in 100 m over the cost (Miramar Beach, 22°17'1,427"N, 97°48'1,271"W). Three samples of 100 mL of seawater were mixed, and the mixture was diluted by a factor of 10000 with distilled water. Again, 100 mL of water was held under constant stirring at 25 °C, and aliquots of 10 mL were taken every 20 min. Samples were diluted to 100 mL, and 1 mL of indicator

solution was added (K_2CrO_4, 0.014 N). Mixtures were titrated with $AgNO_3$ 0.014 N until the change of color from straw yellow to red-orange (Figure 3).

(**a**) (**b**) (**c**)

Figure 3. Water-biofilm interaction method: (**a**) immersion of biofilms for BOD, COD, and Cl^-; sample before (**b**) and after (**c**) titration.

Total chloride was calculated with Equation 5, where A and B represent the mL of $AgNO_3$ used for the sample and the blank, respectively; V is the sample volume (100 mL), and DF is the dilution factor.

$$Cl^- \left(\frac{mg}{L}\right) = \frac{35.453(A-B)}{V} \times DF \quad (5)$$

3. Results and Discussion

3.1. Characteristics of natural extracts.

3.1.1. Total anthocyanins quantification.

Figure 4 shows the UV-Vis spectra obtained for the extracts. For pomegranate, the absorbance value at 535 nm is 0,1081. Therefore, according to Equation 1, the total anthocyanin content from pomegranate is:

$$C_1 = 449 \times 10^6 \frac{g}{mol}\left(\frac{0{,}1081}{25965\frac{1}{M \cdot cm}}\right)\left(\frac{226\,mL}{1000}\right)\left(\frac{1}{4{,}1765\,g}\right) = 101{,}16\frac{mg}{kg} \quad (6)$$

Total anthocyanin in red radish was calculated with Equation 2. In this case, A_2 was determined with the absorbance values at 510 nm for solutions with pH 1 and 4,5.

$$C_2 = \left(1{,}3534 \times 433{,}2\frac{g}{mol} \times 10^3\right)\left(\frac{1}{31600\frac{1}{M \cdot cm} \times 1\,cm}\right) = 18{,}55\frac{mg}{L}\left(\frac{0{,}025\,L}{0{,}0016\,kg}\right) = 289{,}89\frac{mg}{kg} \quad (7)$$

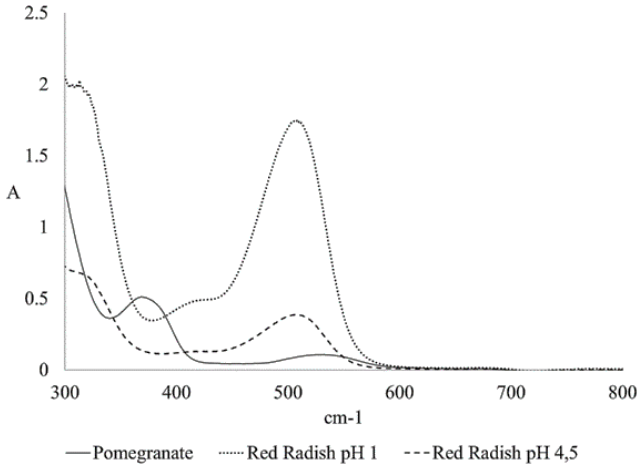

Figure 4. UV-Vis spectra for the total anthocyanin content in pomegranate and red radish.

3.1.2. NMR analysis.

According to the literature, for the ^{1}H and ^{13}C NMR analysis, a descriptors series was first obtained for anthocyanin in pomegranate and red radish. Pomegranate contains pelargonidin, peonidin, and delphinidin; red radish contains cyanidin, malvidin, peonidin, and delphinidin [16,17,22,39-43]. Then, these signals were compared to those observed in the natural extracts. Tables 4 and 5 show the ^{1}H descriptors, and Table 6 shows the ^{13}C descriptors for the base structure of anthocyanins shown in Figure 5 [42].

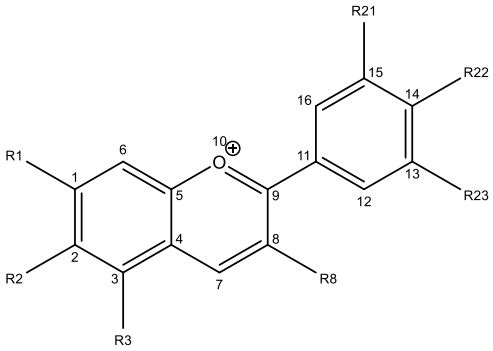

Figure 5. The base structure of anthocyanins.

Table 4. Theoretical profile of the ^{1}H chemical shifts of pomegranate anthocyanins.

Pelargonidin			Peonidin			Delphinidin		
Protons	**Substituent**	**J (Hz)**	**Protons**	**Substituent**	**J (Hz)**	**Protons**	**Substituent**	**J (Hz)**
7H	R8 = OH	s	7H	R8 = OH	d (0,9)	7H	R8 = OH	d (0,9)
2H	R3 = OH	d (1,9)	2H	R3 = OH	d (1,9)	2H	R3 = OH	d (1,9)
1H	R1 = OH	dd (0,9;1,9)	1H	R1 = OH	dd (0,9;1,9)	1H	R1 = OH	dd (0,9;1,9)
16H	R22 = OH	d (8,7)	16H	R22 = OH	d (2,3)	16H	R21 = OH	s
15H		d (8,7)	13H	R21 = OCH_3	d (8,7)	12H	R22 = OH	s
13H		d (8,7)	12H		dd (2,3;8,7)		R23 = OCH_3	
12H		d (8,7)			OCH_3 s			

d = doublet, dd = doubles doublet, s = singlet, J = (coupling constant, Hz)

Table 5. Theoretical profile of the ^{1}H chemical shifts of red radish anthocyanins.

Cyanidin			Malvidin			Peonidin			Delphinidin		
Prot.	**Subst.**	**J (Hz)**	**Prot.**	**Subst.**	**J (Hz)**	**Prot.**	**Subst.**	**J (Hz)**	**Prot.**	**Subst.**	**J (Hz)**
7H	R8=OH	d (0,9)	7H	R8=OH	s	7H	R8=OH	d (0,9)	7H	R8=OH	d (0,9)
2H	R3=OH	d (1,9)	2H	R3=OH	d (1,9)	2H	R3=OH	d (1,9)	2H	R3=OH	d (1,9)
6H	R1=OH	dd (0,9;1,9)	6H	R1=OH	d (1,9)	6H	R1=OH	dd (0,9;1,9)	6H	R1=OH	dd (0,9;1,9)
16H	R21=OH	d (2,3)	16H	R22=OH	s	16H	R22=OH	d (2,3)	16H	R21=OH	s
13H	R22=OH	d (8,7)	12H	R21=OCH_3	s	13H	R21=OCH_3	d (8,7)	12H	R22=OH	s
12H		dd (2,3;8,7)		R23'=OCH_3	OCH_3 s	12H		dd (2,3;8,7)		R23=OCH_3	

d = doublet, dd = doubles doublet, s = singlet, J = (coupling constant, Hz)

Table 6. Theoretical profile of the ^{13}C chemical shifts of pomegranate and red radish anthocyanins.

Position	**Descriptors**				
	Pelargonidin	**Peonidin**	**Delphinidin**	**Cyanidin**	**Malvidin**
1	-C(OH)=	-C(OH)=	-C(OH)=	-C(OH)=	-C(OH)=
2	=C(H)-	=C(H)-	=C(H)-	=C(H)-	=C(H)-
3	-C(OH)=	-C(OH)=	-C(OH)=	-C(OH)=	-C(OH)=
4	=C-	=C-	=C-	=C-	=C-
5	-C=	-C=	-C=	-C=	-C=
6	=C(H)-	=C(H)-	=C(H)-	=C(H)-	=C(H)-
7	=C(H)-	=C(H)-	=C(H)-	=C(H)-	=C(H)-
8	-C(OH)=	-C(OH)=	-C(OH)=	-C(OH)=	-C(OH)=
9	O=C-	O=C-	O=C-	O=C-	O=C-
10	O^{+}	O^{+}	O^{+}	O^{+}	O^{+}

Position	Descriptors				
	Pelargonidin	Peonidin	Delphinidin	Cyanidin	Malvidin
11	-C=	-C=	-C=	-C=	-C=
12	-C(H)=	-C(H)=	-C(H)=	-C(H)=	-C(H)=
13	=C(H)-	=C(H)-	=C(OH)-	=C(H)-	=C(OCH_3)-
14	-C(OH)=	-C(OH)=	-C(OH)=	-C(OH)=	-C(OH)=
15	=C(H)-	=C(OCH_3)-	=C(OH)-	=C(OH)-	=C(OCH_3)-
16	-C(H)=	-C(H)=	-C(H)=	-C(H)=	-C(H)=

Tables 7 and 8 show the results obtained for the natural extracts from the NMR spectra in Figure 6. The anthocyanins' chemical shifts are 0,9, 1,9, and 8,7 ppm, as reported in the literature for ^1H [16,17,22,39-43]. The extracts do not observe such signals because the high sugar content generates more intense signals. However, for red radish, one of the characteristic signals at 1,9 ppm is observed besides the signals of aromatic compounds at 6 and 9 ppm. These chemical shifts could be related to the total anthocyanin content that is higher in red radish than in pomegranate, and therefore, pomegranate has higher sugar content. This is also observed in ^{13}C analysis, where the characteristic chemical shifts are between 95 and 165 ppm. Hence, anthocyanins' presence is partially confirmed without a purification process required.

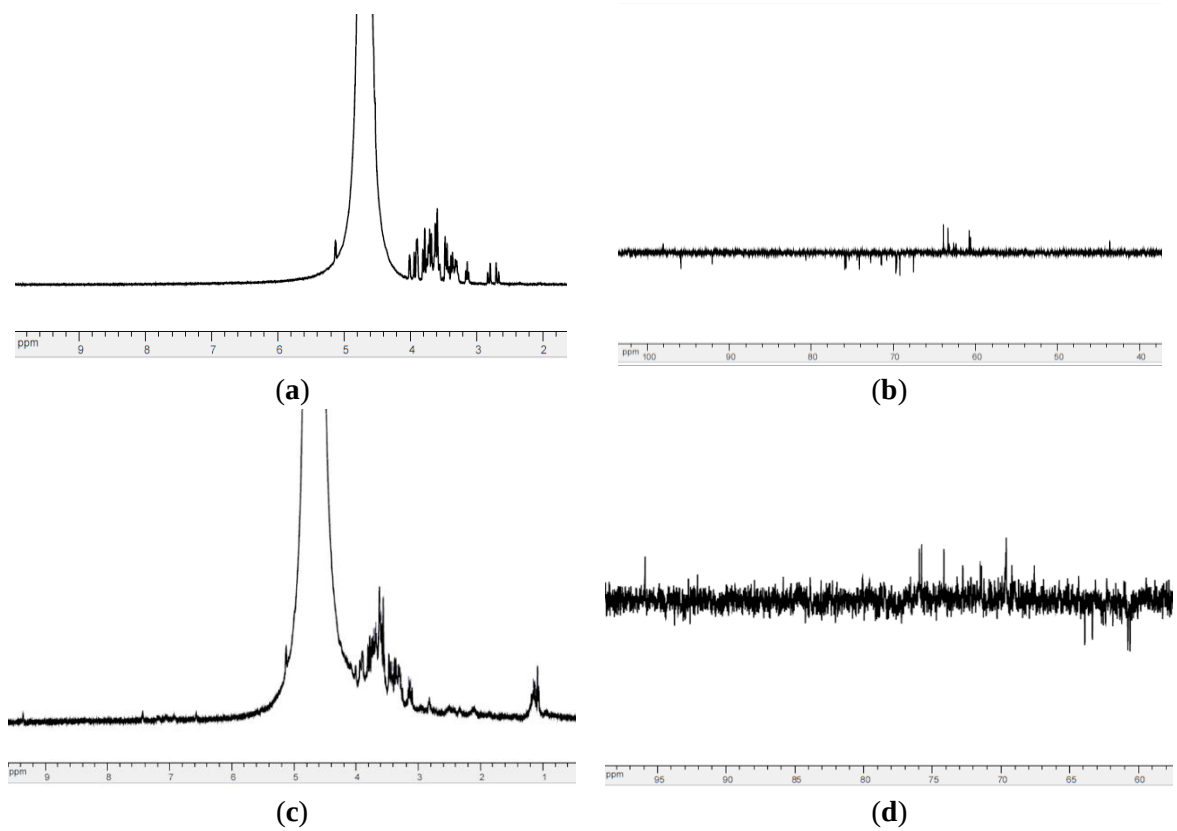

Figure 6. NMR spectra obtained: (**a**)^1H and (**b**)^{13}C for pomegranate; (**c**)^1H and (**d**)^{13}C for red radish.

Table 7. ^1H chemical shifts in pomegranate and red radish extracts.

δ (ppm)	Multiplicity	Assignation
Pomegranate		
2,665 – 2,832	dd	CH_3-C=O, CH_3-S-, CH_3-N=, H-C≡C-
3,12 – 3,163	t	H-C≡C-, ArSH, R-OH
3,288 – 3,476	m (13)	H-C≡C-, ArSH, R-OH, CH_3-O-, $ArNH_2$, ArNHR, Ar_2NH
3,512	s	Sugars, ArSH, R-O, CH_3-O-, $ArNH_2$, ArNHR, Ar_2NH
3,553 – 3,812	m (17)	Sugars, ArSH, R-OH, CH_3-O-, $ArNH_2$, ArNHR, Ar_2NH
3,895 – 4,013	m (4)	Sugars, ArSH, R-OH, CH_3-O-, $ArNH_2$, ArNHR, Ar_2NH
Red Radish		
1,065 – 1,183	m (7)	CH_3-C-, R_2NH, CH_3-C-C-X, -C-H
1,992	s	R_2NH, CH_3-C-C-X, CH_3-C=C

δ (ppm)	Multiplicity	Assignation
2,118 – 2,2	t	R_2NH, CH_3-C≡C
2,336 – 2,43	t	R_2NH, CH_3-C≡C, CH_3-Ar, CH-S, CH-N
2,502 – 2,602	m (4)	CH_3-C≡C, CH_3-Ar, CH-S, CH-N
2,825	d	H-C≡C-
3,104 – 3,161	m (4)	H-C≡C-, $ArNH_2$, ArNHR, Ar_2NH
3,256 – 3,477	m (10)	H-C≡C-, ArSH, R-OH, CH_3-O-, $ArNH_2$, ArNHR, Ar_2NH
3,53 – 3,813	m (14)	Sugars, H-C≡C-, ArSH, R-OH, CH_3-O-, $ArNH_2$, ArNHR, Ar_2NH
3,903 – 3,942	d	Sugars, H-C≡C-, ArSH, R-OH, CH_3-O-, $ArNH_2$, ArNHR, Ar_2NH
4,012	s	Sugars, CH_3-O-
6,577	s	6H, CH_2=C-, ArOH, HC=C-, H-N-C=O, ArH
6,943 – 7,189	t	8H, ArOH, HC=C-, H-N-C=O, ArH
7,436	s	2H, ArOH, HC=C-, H-N-C=O, ArH
9,361	s	4H, $ArNH_3$, $ArRNH_2$, ArR_2NH, -C=N

Table 8. ^{13}C chemical shifts observed in pomegranate and red radish extracts.

δ (ppm)	Assignation
Pomegranate	
101,437	-C=C-
98,074	-C=C- -C≡C-
95,919	=C(H)- -C=C- -C≡C-
92,099	-C=C- -C≡C-
80,67 – 67,569	-C=C- -C≡C- =CH-O $-CH_2$-O CH-Hal C-Hal -CH-N
63,897 – 60,598	-CH- $-O-CH_3$ CH_2-O CH-Hal C-Hal C-N CH-N
43,636	$-CH_2$- CH-N- $-CH_2$-N- CH_3-N- -CH-C- -C-C- -CH-Hal -C-Hal
Red Radish	
95,919	=C(H)- -C=C- -C≡C-
75,783	-C=C- -C≡C-
75,945	-C=C- -C≡C-
74,169	-C=C- -C≡C-
72,785 – 67,576	-C=C- -C≡C- =CH-O $-CH_2$-O CH-Hal C-Hal -CH-N
63,904 – 60,612	-CH- O-CH_3 CH_2-O CH-Hal C-Hal C-N CH-N

3.2. Characterization of biofilms.

3.2.1. Rheology of CSA and CSF biofilm precursors.

The rheological behavior of the biofilm precursor mixtures was studied to determine their flowability in terms of viscosity at different temperatures. As shown in Figure 7, both combinations present a Newtonian behavior, corresponding to the linear viscosity decrease as the temperature increases (Figure 8). This is a common characteristic of polymer solutions [44] and does not compromise the physicochemical properties of the chitosan-starch blends studied in this work.

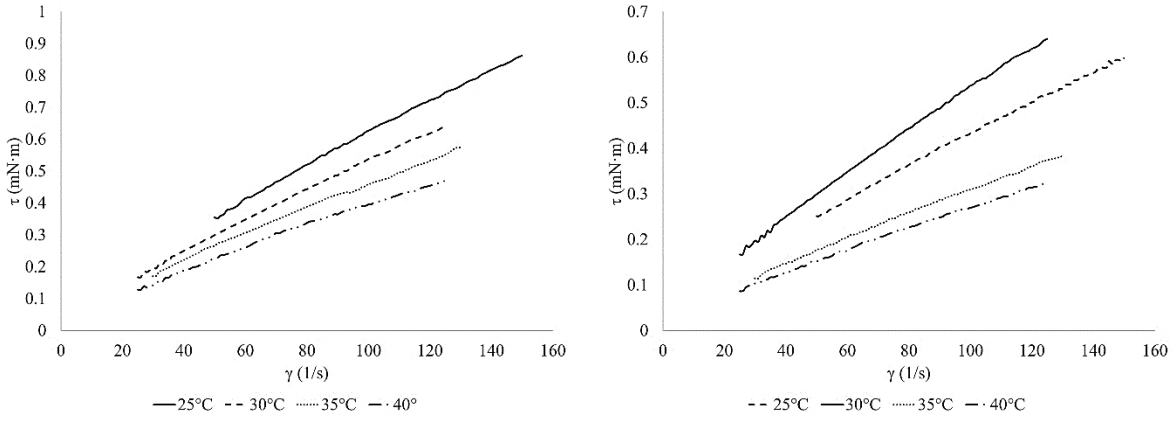

Figure 7. Rheological behavior of (**a**) CSA and (**b**) CSF solutions for a shear rate (γ) range from 20 to 150 1/s at different temperature values.

However, it is essential to note that combinations with acetic acid presented a higher viscosity value, which can be related to a better fluid consistency. Such physical observation of the precursor mixture indicates the biofilms' possible mechanical behavior.

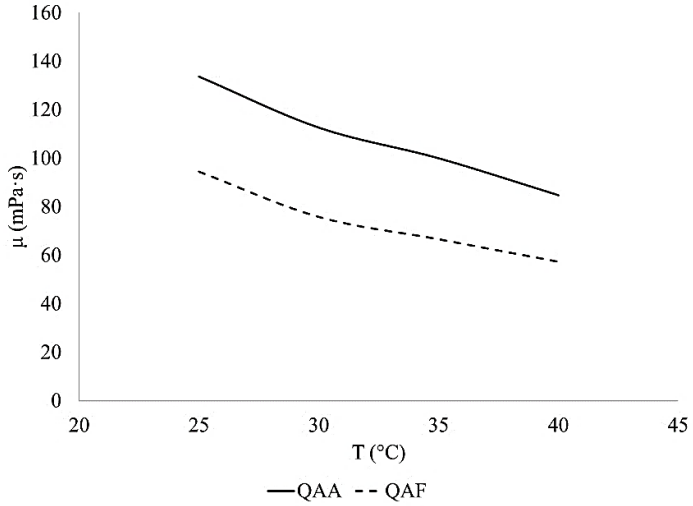

Figure 8. Viscosity **(μ)** behavior of CSA and CSF solutions from 25 to 40 °C for a share rate **(γ)** of 50 1/s.

3.2.2. Thickness and tensile strength measurement.

Figure 4 shows the biofilms obtained. A brown color tendency with pomegranate extract addition can be observed, and it is slightly boosted in those films produced with formic acid. Table 9 shows the results of thickness and tensile strength tests. It can be observed that the use of different acids to promote the chitosan-starch assembly has an impact on mechanical behavior.

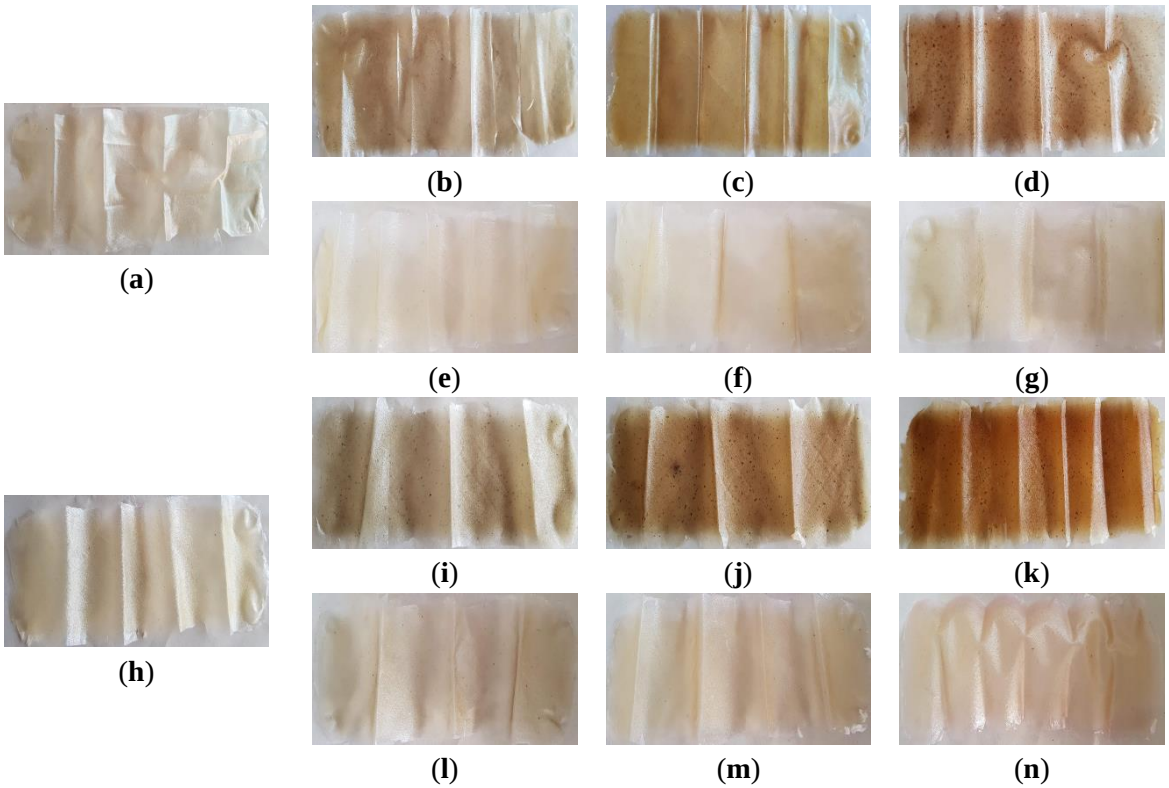

Figure 9. Biofilms samples obtained: (**a**) CSA, (**b**) CSAP0,5 (**c**) CSAP2, (**d**) CSAP5, (**e**) CSAR0,5 (**f**) CSAR2, (**g**) CSAR5, (**h**) CSF, (**i**) CSFP0,5 (**j**) CSFP2, (**k**) CSFP5, (**l**) CSFR0,5 (**m**) CSFR2, (**n**) CSFR5.

A higher level of acidity allows a faster integration of the materials, but once the moisture has been removed, the acid promotes a quicker degradation of the film. Therefore, the modulation of acidity levels in the aqueous solution is crucial to modulating the biofilm's mechanical properties.

Table 9. Thickness and tensile strength of the biofilms.

ID	Thickness (mm)	Tensile strength (MPa)
CSA	0,0393 ± 0,0064	62,37
CSAP0,5	0,036 ± 0,0104	63,73
CSAP2	0,0373 ± 0,0023	67,03
CSAP5	0,0367 ± 0,005	62,9
CSAR0,5	0,066 ± 0,002	67,52
CSAR2	0,0453 ± 0,0092	69,99
CSAR5	0,04 ± 0,004	68,81
CSF	0,0567 ± 0,0061	35,59
CSFP0,5	0,0433 ± 0,0092	34,12
CSFP2	0,0553 ± 0,0076	34,23
CSFP5	0,0633 ± 0,0012	31,17
CSFR0,5	0,046 ± 0,0072	33,68
CSFR2	0,0553 ± 0,0064	31,92
CSFR5	0,0507 ± 0,0117	35,94

3.2.3. Accelerated weathering test.

The general physical quality of the biofilms was tested under accelerated weathering conditions. The mass and physical state were measured before and after, and the results are recorded in Table 10. For some samples, there is an increase in weight, which is referred to as the moisture absorbed. Also, for some of these films, the effect of the water absorbed is reflected in the final physical state. In general terms, the impact of using formic acid on tensile strength is confirmed by the last physical condition after the weathering test. Besides, it is observed that the moisture is desorbed for most of the films produced with formic acid. Such behavior supports the idea that acidity affects the physical properties of the films determined from the precursor mixture. A microscopy test with polarizable light was carried out to evaluate the surface characteristics of the biofilms before and after the weathering test. It is observed that after the test, all the surfaces present a smoothing, black zones, and microfractures appearance related to the UV light attack. The results are observed in Figure 10.

Table 10. The initial and final condition of biofilms under accelerated weathering.

ID	Initial mass (g)	Initial physical state	Final mass (g)	Final physical state
CSA	1,9697	Flexible	2,1588	Flexible
CSAP0,5	1,8401	Flexible	1,5139	Flexible
CSAP2	1,9262	Flexible	1,7205	Semirigid
CSAP5	2,1224	Flexible	2,006	Semirigid
CSAR0,5	2,173	Flexible	2,153	Flexible
CSAR2	2,1518	Flexible	2,281	Low flexibility
CSAR5	1,8928	Flexible	1,9679	Rigid, brittle to the touch
CSF	2,1604	Flexible	2,2	Rigid, brittle to the touch
CSFP0,5	1,9812	Flexible	1,7749	Flexible
CSFP2	2,1759	Flexible	2,1225	Rigid, brittle to the touch
CSFP5	2,1586	Flexible	2,261	Rigid, brittle to the touch
CSFR0,5	1,9791	Flexible	1,7248	Semirigid
CSFR2	1,9798	Flexible	1,9285	Semirigid
CSFR5	1,9581	Flexible	1,7272	Semirigid

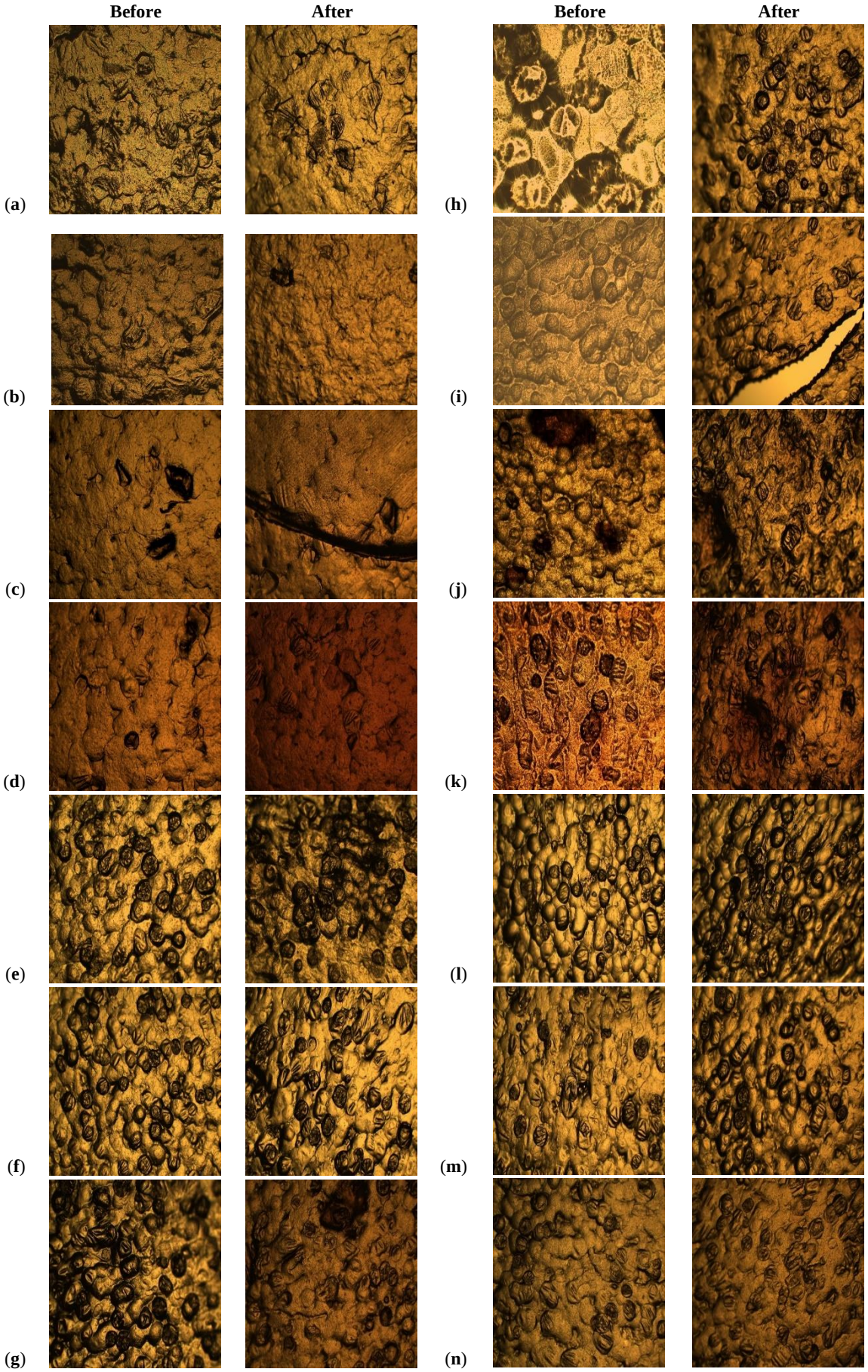

Figure 10. Micrographic before and after weathering test: (**a**) CSA, (**b**) CSAP05, (**c**) CSAP2, (**d**) CSAP5, (**e**) CSAR0,5 (**f**) CSAR2, (**g**) CSAR5, (**h**) CSF, (**i**) CSFP0,5 (**j**) CSFP2, (**k**) CSFP5, (**l**) CSFR0,5 (**m**) CSFR2, (**n**) CSFR5.

3.3. Application results.

3.3.1. Antimicrobial activity.

Table 11 shows the antimicrobial activity results. It is observed that once more, the type of acid employed in the formulation tends to lead to the behavior studied. In this case, the effect is opposite to the mechanical properties, as the formic acid promotes an inhibition halo that reduces the attack and infestation of microorganisms in the films produced. However, it is also observed that red radish extract increases the effectivity of the films for this parameter for fungi and total coliforms. Pomegranate works better against aerobic mesophilic, implying that the anthocyanins in the source are selective according to the microbiota. It is important to note that the highest content of red radish extract equals the pomegranate activity. Therefore both are suitable for antimicrobial applications.

Table 11. Antimicrobial activity of the sample films with an initial diameter of 0,6 cm.

	Fungi		**Total coliforms**		**Aerobic mesophilic**	
ID	**d_{final} (cm)**	**d_{halo} (cm)**	**d_{final} (cm)**	**d_{halo} (cm)**	**d_{final} (cm)**	**d_{halo} (cm)**
CSA	0,8	---	0,8	---	0,7	---
CSAP0,5	0,9	1	0,7	1,2	0,8	0,9
CSAP2	0,8	---	0,7	---	0,7	---
CSAP5	0,7	---	0,6	---	0,6	---
CSAR0,5	0,8	---	0,7	1	0,8	---
CSAR2	0,8	---	0,8	1	0,8	---
CSAR5	0,8	---	0,7	0,9	0,8	---
CSF	1	---	1	---	0,9	---
CSFP0,5	1	1,7	1	1,4	0,9	1,1
CSFP2	0,9	1,2	0,8	0,9	0,9	1,1
CSFP5	0,8	0,9	0,7	0,8	0,7	0,9
CSFR0,5	0,8	1,2	0,9	---	1	---
CSFR2	1	1,5	1,2	1,7	1	---
CSFR5	0,9	1,2	1	1,1	1	1,2

3.3.2. BOD and COD reduction activity.

The reduction activity of BOD and COD was evaluated to compare the antimicrobial behavior of the biofilms. It was observed that both extracts, no matter what acid was used, affected the retention of organic material.

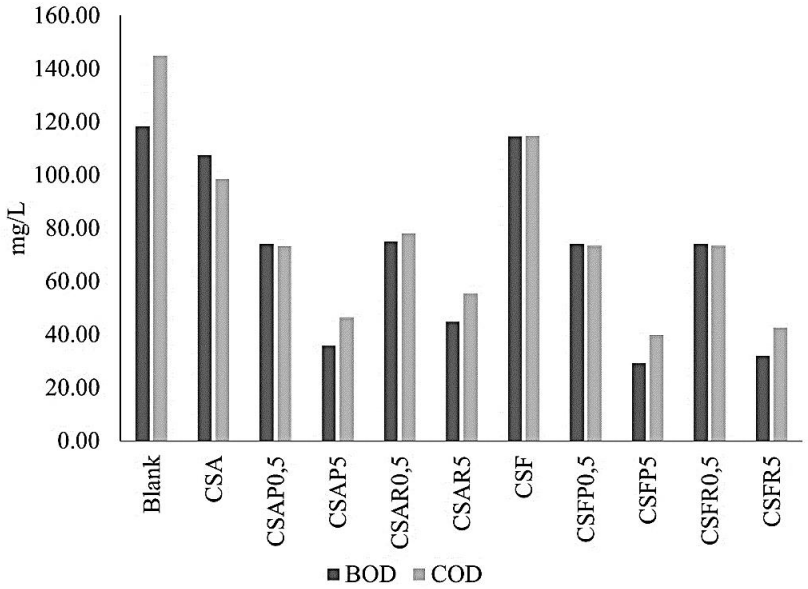

Figure 11. BOD and COD reduction activity of the biofilms.

As observed in Figure 11, the films without organic extracts showed a remotion activity that improved with the addition of the organic materials and increased as the extract increased. This could be related to a simple surface adsorption process; however, the antimicrobial activity indicates that extracts have a selectivity to organic residues or microbiota. Such behavior is ideal for water remediation, and the formulations developed suit water treatment technologies. For this test and chloride ion remotion activity, only the highest and the lowest concentration of organic extract were analyzed to observe the behavior of the concentration limits studied in this work.

3.3.3. Chloride ion remotion activity.

The water absorption observed in the accelerated weathering test was taken advantage of for ion chloride retention. The results are shown in Figures 12 and 13. It is observed that both formic and acetic acids retent chloride by themselves; however, the presence of anthocyanins produces a faster retention activity in the presence of formic acid. This behavior can be associated with the dual effect of anthocyanin/formic acid according to the active sites in their structures to interact with Na^+ and Cl^- ions.

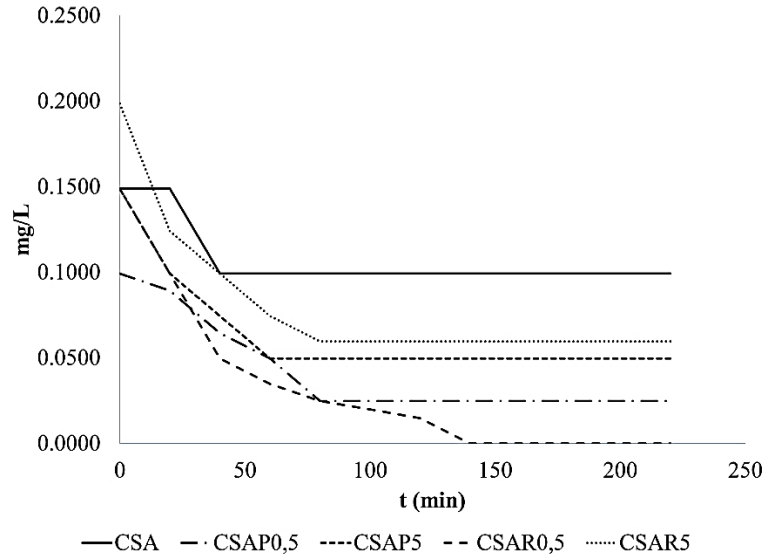

Figure 12. Chloride ion remotion activity of CSA biofilms series.

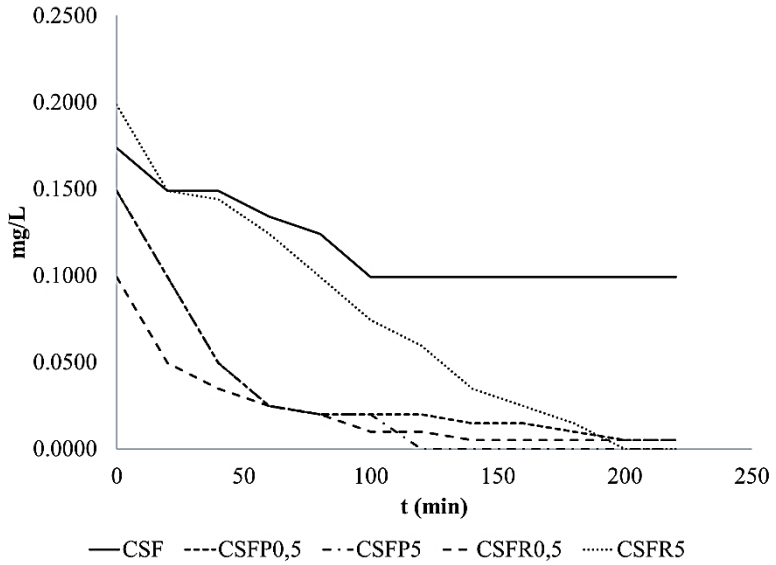

Figure 13. Chloride ion remotion activity of CSF biofilms series.

From the results observed with NaCl aqueous solution, the biofilms with the best ion interaction performance in terms of time were tested with seawater. The biofilms selected were CSFR5, CSFP5, and CSAR0,5, and similar behavior was observed. The results are shown in Figure 14, and this indicates that even in the presence of other ions (from the different salts in seawater), the biofilms performed good retention of the chloride ion proposed in this work.

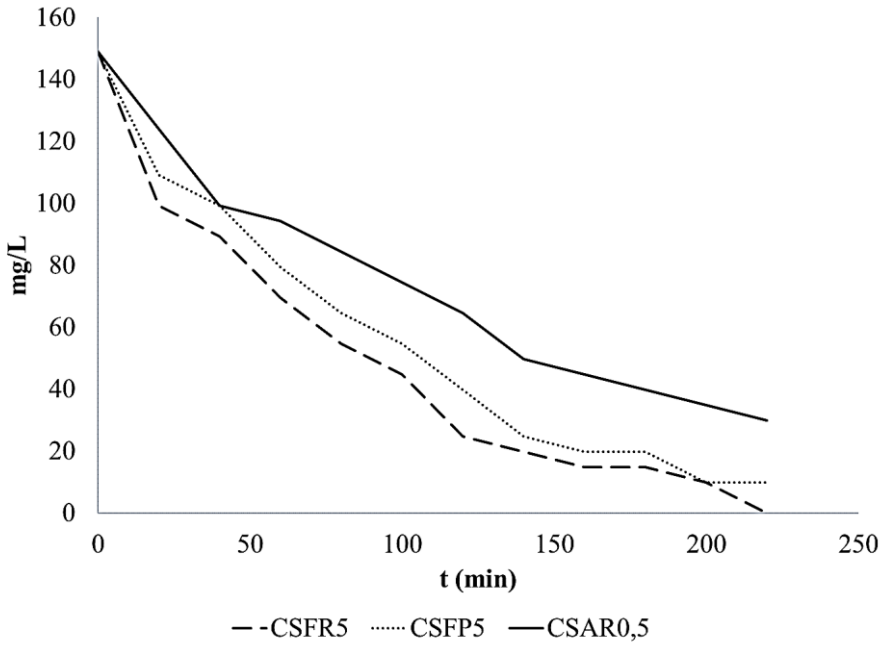

Figure 14. Chloride ion remotion activity in seawater.

4. Conclusions

This work produced a series of chitosan-starch films and added them with pomegranate and red radish extracts. The biofilms were prepared from blends with two different acids, formic and acetic, to observe the effect on the integration of the materials. It was found that the type of acid affects the mechanical properties, and Acetic acid produces films with higher tensile strength and weathering resistance. However, in combination with anthocyanins from the natural extracts, formic acid performs a better antimicrobial activity and BOD and COD control. This behavior is improved with the use of the red radish extract.

On the other hand, the chloride ion interaction test had better results (even in the presence of other ions) for those films produced with formic acid. Therefore, in terms of applicability, future work should be focused on the pursuit of formulations mixing the four elements: formic acid, acetic acid, red radish extract, and pomegranate extract, based on the extraction process employed in this work as it demonstrated the extraction of anthocyanins according to the characterization tests. In this way, what should be improved is the resistance of the biofilms that allow their use in purification methods or systems (like filters or membrane beds), and it is expected that antimicrobial activity, retention of organic material, and interaction with salts ions were improved for achieving water treatment at large scale.

Funding

This research received no external funding.

Acknowledgments

MNMR thanks Centro de Investigación en Petroquímica and Centro de Investigación FADU UAT for their facilities, reactants, and equipment. Also, a special acknowledgment to ITCM Campus 1 for access to the Microbiology Laboratory.

Conflicts of Interest

The authors declare no conflict of interest.

References

1. Wheeler, S. A. Lessons from water markets around the world. In *Water Markets*, 1st ed.; Wheeler, S.A., Ed.; Edward Elgar Publishing: Cheltenham, United Kingdom, **2021**, pp. 235-251, https://doi.org/10.4337/9781788976930.00024.
2. Kammeyer, C.; Hamilton, R.; Morrison, J. Averting the global water crisis: three considerations for a new decade of water governance. *Georgetown J Int Aff* **2020**, *21*, 105-113, https://doi.org/10.1353/gia.2020.0026.
3. Sauvé, S., Lamontagne, S., Dupras, J., Stahel, W. Circular economy of water: Tackling quantity, quality, and footprint of water. *Environ Dev* **2021**, *39*, 100651, https://doi.org/10.1016/j.envdev.2021.100651.
4. Assaf, A. T.; Sayl, K. N.; Adham, A. Surface water detection method for water resources management. In *Journal of Physics: Conference Series*, *Proceeding of the 3rd International Scientific Conference of Engineering Sciences and Advances Technologies (IICESAT), College of Material Engineering, University of Babylon, Iraq, 4-5 June 2021*; IOP Publishing Limited: Bristol, United Kingdom, **2021**, *1973*, 012149, https://doi.org/10.1088/1742-6596/1973/1/012149.
5. Bozorg-Haddad, O.; Zolghadr-Asli, B.; Sarzaeim, P.; Aboutalebi, M.; Chu, X.; Loáiciga, H. A. Evaluation of water shortage crisis in the Middle East and possible remedies. *J Water Supply: Res Technol AQUA* **2020**, *69*, 85-98, https://doi.org/10.2166/aqua.2019.049.
6. Mexico's water and sanitation crisis. https://water.org/our-impact/where-we-work/mexico/.
7. CONAGUA apoyará rehabilitación del dique El Camalote, en Tamaulipas. Available online: https://www.gob.mx/conagua/prensa/conagua-apoyara-rehabilitacion-del-dique-el-camalote-en-tamaulipas.
8. Yusuf, A.; Sodiq, A.; Giwa, A.; Eke, J.; Pikuda, O.; De Luca, G.; Luque Di Salvo, J.; Chakraborty, S. A review of emerging trends in membrane science and technology for sustainable water treatment. *J Clean Prod* **2020**, *266*, 121867, https://doi.org/10.1016/j.jclepro.2020.121867.
9. Mukhopadhyay, R.; Bhaduri, D.; Sarkar, B.; Rusmin, R.; Hou, D.; Khanam, R.; Sarkar, S.; Biswas, J.K.; Vithanage, M.; Bhatnagar, A.; Ok, Y. S. Clay–polymer nanocomposites: Progress and challenges for use in sustainable water treatment. *J Hazard Mater* **2020**, *383*, 121125, https://doi.org/10.1016/j.jhazmat.2019.121125.
10. Nasrollahzadeh, M.; Sajjadi, M.; Iravani, S.; Varma, R. S. Starch, cellulose, pectin, gum, alginate, chitin, and chitosan derived (nano) materials for sustainable water treatment: A review. *Carbohydr Polym* **2020**, *251*, 116986, https://doi.org/10.1016/j.carbpol.2020.116986.
11. Mehdizadeh, T.; Tajik, H.; Langroodi, A. M.; Molaei, R.; Mahmoudian, A. Chitosan-starch film containing pomegranate peel extract and Thymus kotschyanus essential oil can prolong the shelf life of beef. *Meat Sci* **2020**, *163*, 108073, https://doi.org/10.1016/j.meatsci.2020.108073.
12. Saiful, S.; Ajrina, M.; Wibisono, Y.; Marlina, M. Development of chitosan/starch-based forward osmosis water filtration bags for emergency water supply. *Membranes* **2020**, *10*, 414, https://doi.org/10.3390/membranes10120414.
13. Han, Y.; Chen, S.; Yang, M.; Zou, H.; Zhang, Y. Inorganic matter modified water-based copolymer prepared by chitosan-starch-CMC-Na-PVAL as an environment-friendly coating material. *Carbohydr Polym* **2020**, *234*, 115925, https://doi.org/10.1016/j.carbpol.2020.115925.
14. Meng, W.; Shi, J.; Zhang, X.; Lian, H.; Wang, Q.; Peng, Y. Effects of peanut shell and skin extracts on the antioxidant ability, physical and structure properties of starch-chitosan active packaging films. *Int J Biol Macromol* **2020**, *152*, 137-146, https://doi.org/10.1016/j.ijbiomac.2020.02.235.
15. Chayavanich, K.; Thiraphibundet, P.; Imyim, A. Biocompatible film sensors containing red radish extract for meat spoilage observation. *Spectrochim Acta A Mol Biomol Spectrosc* **2020**, *226*, 117601, https://doi.org/10.1016/j.saa.2019.117601.

16. Roy, S.; Rhim, J.W. Anthocyanin food colorant and its application in pH-responsive color change indicator films. *Crit Rev Food Sci Nutr* **2020**, 2297-2325, https://doi.org/10.1080/10408398.2020.1776211.
17. Dias, S.; Castanheira, E.; Fortes, A. G.; Pereira, D. M.; Gonçalves, M. S. T. Natural pigments of anthocyanin and betalain for coloring soy-based yogurt alternative. *Foods* **2020**, *9*, 771, https://doi.org/10.3390/foods9060771.
18. Halonen, N., Pálvölgyi, P.S.; Bassani, A.; Fiorentini, C.; Nair, R.; Spigno, G.; Kordas, K. Bio-based smart materials for food packaging and sensors–A Review. *Front Mater* **2020**, *7*, https://doi.org/10.3389/fmats.2020.00082.
19. Luzardo-Ocampo, I.; Ramírez-Jiménez, A. K.; Yañez, J.; Mojica, L.; Luna-Vital, D. A. Technological applications of natural colorants in food systems: A Review. *Foods* **2021**, *10*, 634, https://doi.org/10.3390/foods10030634.
20. Priyadarshi, R.; Ezati, P.; Rhim, J. W. Recent advances in intelligent food packaging applications using natural food colorants. *ACS Food Sci Technol* **2021**, *1*, 124-138, https://doi.org/10.1021/acsfoodscitech.0c00039.
21. Rastogi, N. K. Applications of forward osmosis process in food processing and future implications. In *Current Trends and Future Developments on (Bio-) Membranes, Reverse and Forward Osmosis: Principles, Applications, Advances, Part 2*, 1st ed.; Basile, A., Cassano, A., Rastogi, N.K., Eds.; Elsevier: Amsterdam, Netherlands, **2020**, pp. 113-138, https://doi.org/10.1016/B978-0-12-816777-9.00005-8.
22. Milla, P.G.; Peñalver, R.; Nieto, G. Health Benefits of Uses and Applications of Moringa oleifera in Bakery Products. *Plants* **2021**, *10*, 318, https://doi.org/10.3390/plants10020318.
23. Frías-Moreno, M. N.; Parra-Quezada, R. A.; González-Aguilar, G.; Ruíz-Canizales, J.; Molina-Corral, F. J.; Sepulveda, D. R.; Salas-Salazar, N.; Olivas, G. I. Quality, Bioactive compounds, antioxidant capacity, and enzymes of raspberries at different maturity stages, effects of organic vs. conventional fertilization. *Foods* **2021**, *10*, 953, https://doi.org/10.3390/foods10050953.
24. Singh, A.; Sharma, S. Radish. In *Antioxidants in Vegetables and Nuts-Properties and Health Benefits*, 1st ed.; Nayik, G.A., Gull, A., Eds.; Springer: Singapore, **2020**; pp. 209-235, https://link.springer.com/book/10.1007/978-981-15-7470-2.
25. Juárez-Méndez, M. E.; Lozano-Navarro, J. I.; Velasco-Santos, C.; Pérez-Sánchez, J. F.; Zapién-Castillo, S.; Del Angel-Moxica, I. E.; Melo-Banda, J. A.; Tijerina-Ramos, B. I.; Díaz-Zavala, N. P. Effect of the Melicoccus bijugatus leaf and fruit extracts and acidic solvents on the antimicrobial properties of chitosan–starch films. *J Appl Microbiol* **2021**, *131*, 1162-1176, https://doi.org/10.1111/jam.15025.
26. Lozano-Navarro, J. I.; Diaz-Zavala, N. P.; Melo-Banda, J. A.; Velasco-Santos, C.; Paraguay-Delgado, F.; Perez-Sanchez, J. F.; Domínguez-Esquivel, J. M.; Suárez-Domínguez, E. J.; Sosa-Sevilla, J. E. Chitosan–Starch Films Modified with Natural Extracts to Remove Heavy Oil from Water. *Water* **2020**, *12*, 17, https://doi.org/10.3390/w12010017.
27. Cazón, P., Velázquez, G., Vázquez, M. Bacterial cellulose films: Evaluation of the water interaction. *Food Packag Shelf Life* **2020**, *25*, 100526, https://doi.org/10.1016/j.fpsl.2020.100526.
28. Udayakumar, G. P.; Muthusamy, S.; Selvaganesh, B.; Sivarajasekar, N.; Rambabu, K.; Banat, F.; Sivamani, S.; Sivakumar, N.; Show, P. L. Biopolymers and composites: Properties, characterization and their applications in food, medical and pharmaceutical industries. *J Environ Chem Eng* **2021**, *9*, 105322, https://doi.org/10.1016/j.jece.2021.105322.
29. Branysova, T.; Demnerova, K.; Durovic, M.; Stiborova, H. Microbial biodeterioration of cultural heritage and identification of the active agents over the last two decades. *J Cult Herit* **2022**, *55*, 245-260, https://doi.org/10.1016/j.culher.2022.03.013.
30. Pardo, L.; Arias, J.; Molleda, P. Preparation of synthesized silver nanoparticles from extract of rosemary leaves (Rosmarinus officinalis L.) and its use as a preservative. *LA GRANJA. Revista de Ciencias de la Vida* **2022**, *35*, 45-58, https://doi.org/10.17163/lgr.n35.2022.04.
31. NOM-092-SSA1-1994, Method for aerobic bacteria count in a plate: Mexican Official Standard, http://www.dof.gob.mx/nota_detalle.php?codigo=4886029&fecha=12/12/1995#:~:text=expide%20la%20siguiente%3A-,NORMA%20OFICIAL%20MEXICANA%20NOM%2D092%2DSSA1%2D1994%2C%20BIENES,DE%20BACTERIAS%20AEROBIAS%20EN%20PLACA.&text=Cuando%20se%20requiere%20investigar%20el,es%20la%20cuenta%20en%20placa.
32. NOM-113-SSA1-1994, Plate count method for Total Coliform Microorganisms: Mexican Official Standard,: http://www.fao.org/faolex/results/details/es/c/LEX-FAOC013519/.

33. NOM-111-SSA1-1994, Method for counting Molds and Yeasts in Foods: Mexican Official Standard,: http://www.fao.org/faolex/results/details/es/c/LEX-FAOC013521/.
34. NMX-AA-003-1980, Guidelines for sampling wastewater discharges: Mexican Standard, http://www.fao.org/faolex/results/details/es/c/LEX-FAOC051790/.
35. NMX-AA-014-1980, Guidelines for sampling in surface water receiving bodies: Mexican Standard, http://www.fao.org/faolex/results/details/es/c/LEX-FAOC051857/.
36. NMX-AA-028-SCFI-2001, Water analysis - Determination for biochemical oxygen demand in natural, wastewaters and wastewaters treated - Test method: Mexican Standard, http://www.fao.org/faolex/results/details/es/c/LEX-FAOC052028/.
37. NMX-AA-030-SCFI-2001, Water analysis - Determination for chemical oxygen demand in natural, wastewaters and wastewaters treated - Test method: Mexican Standard, https://agua.org.mx/wp-content/uploads/2011/01/nmx-aa-030-scfi-2001.pdf.
38. NMX-AA-073-SCFI-2001, Water analysis - Determination of total chlorine in natural water, wastewaters, and wastewaters treated - Test method: Mexican Standard, https://www.gob.mx/cms/uploads/attachment/file/166789/NMX-AA-073-SCFI-2001.pdf.
39. Li, B.; Wang, L.; Bai, W.; Chen, W.; Chen, F.; Shu, C. *Anthocyanins: Chemistry, Processing and Bioactivity*, 1st ed.; Springer: Singapore, **2021**, pp. 53-73.
40. Thajai, N.; Jantanasakulwong, K.; Rachtanapun, P.; Jantrawut, P.; Kiattipornpithak, K.; Kanthiya, T.; Punyodom, W. Effect of chlorhexidine gluconate on mechanical and antimicrobial properties of thermoplastic cassava starch. *Carbohydr Polym* **2022**, *275*, 118690, https://doi.org/10.1016/j.carbpol.2021.118690.
41. Macedo, E. H. B.; Santos Jr, G. C.; Santana, M. N.; Jesus, E. F. O.; de Araújo, U. B.; Anjos, M. J.; Pinhero, A.S.; Carneiro, C.S.; Rodrigues, I. A. Unveiling the physicochemical properties and chemical profile of artisanal jabuticaba wines by bromatological and NMR-based metabolomics approaches. *LWT Food Sci Technol* **2021**, *146*, 111371, https://doi.org/10.1016/j.lwt.2021.111371.
42. Karantzi, A. D.; Kafkaletou, M.; Christopoulos, M. V.; Tsantili, E. Peel color and flesh phenolic compounds at ripening stages in pollinated commercial varieties of fig (Ficus carica L.) fruit grown in Southern Europe. *J Food Meas Charact* **2021**, *15*, 2049-2063, https://doi.org/10.1007/s11694-020-00796-4.
43. Enaru, B.; Drețcanu, G.; Pop, T. D.; Stănilă, A.; Diaconeasa, Z. Anthocyanins: Factors affecting their stability and degradation. *Antioxidants* **2021**, *10*, 1967, https://doi.org/10.3390/antiox10121967.
44. Polymer Properties Database. Flow properties of polymers: time-independent fluids, https://polymerdatabase.com/polymer%20physics/Viscosity2.html.